JACS
JOURNAL OF THE AMERICAN CHEMICAL SOCIETY

Article

pubs.acs.org/JACS

Visualization of Steady-State Ionic Concentration Profiles Formed in Electrolytes during Li-Ion Battery Operation and Determination of Mass-Transport Properties by *in Situ* Magnetic Resonance Imaging

Sergey A. Krachkovskiy,[†] J. David Bazak,[†] Peter Werhun,[†] Bruce J. Balcom,[‡] Ion C. Halalay,[§] and Gillian R. Goward*[,†]

[†]Department of Chemistry, McMaster University, Hamilton, Ontario, Canada L8S 4L8

[‡]Department of Physics, University of New Brunswick, Fredericton, New Brunswick, Canada E3B 5A3

[§]General Motors Global Research and Development, 30500 Mound Road, Warren, Michigan 48092-2031, United States

Supporting Information

ABSTRACT: Accurate modeling of Li-ion batteries performance, particularly during the transient conditions experienced in automotive applications, requires knowledge of electrolyte transport properties (ionic conductivity κ, salt diffusivity D, and lithium ion transference number t^+) over a wide range of salt concentrations and temperatures. While specific conductivity data can be easily obtained with modern computerized instrumentation, this is not the case for D and t^+. A combination of NMR and MRI techniques was used to solve the problem. The main advantage of such an approach over classical electrochemical methods is its ability to provide spatially resolved details regarding the chemical and dynamic features of charged species in solution, hence the ability to present a more accurate characterization of processes in an electrolyte under operational conditions. We demonstrate herein data on ion transport properties (D and t^+) of concentrated $LiPF_6$ solutions in a binary ethylene carbonate (EC)−dimethyl carbonate (DMC) 1:1 v/v solvent mixture, obtained by the proposed technique. The buildup of steady-state (time-invariant) ion concentration profiles during galvanostatic experiments with graphite−lithium metal cells containing the electrolyte was monitored by pure phase-encoding single point imaging MRI. We then derived the salt diffusivity and Li^+ transference number over the salt concentration range 0.78−1.27 M from a pseudo-3D combined PFG-NMR and MRI technique. The results obtained with our novel methodology agree with those obtained by electrochemical methods, but in contrast to them, the concentration dependences of salt diffusivity and Li^+ transference number were obtained simultaneously within the single *in situ* experiment.

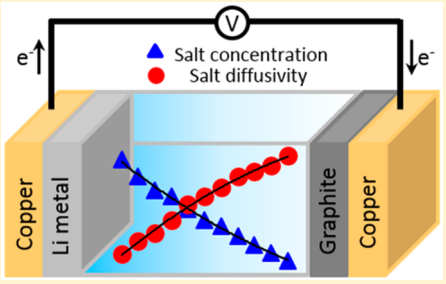

INTRODUCTION

The operation of battery management systems requires that the transient conditions experienced by a battery cell in electrified vehicle applications can be accurately described through battery modeling.[1] The accurate parametrization of the lithium ion transport in electrolyte solutions is a critical component of any battery model (whether at atomic, particulate, or continuum length scales) aiming to achieve such a task. Nyman et al. showed that, when a battery undergoes an HPPC (hybrid pulse power characterization) test, over 40% of the processes leading to cell polarization are related to electrolyte transport effects.[2] Electrolyte solutions can experience large concentration polarizations, due to comparatively low values of the Li^+ cation transference number (t^+) and the salt diffusivity (D), particularly during battery operation at high charge/discharge rates and/or at low temperatures. Reliable data on the transport properties of electrolyte solutions, as functions of both salt concentration and temperature, are therefore a prerequisite for accurate electrochemical modeling.

It was shown recently that magnetic resonance imaging (MRI) can serve as a powerful, noninvasive tool for monitoring the performance of materials in energy storage and power devices (lithium-ion batteries, double-layer capacitors, and fuel cells).[3−6] *In situ* MRI has been used to visualize the spatial distribution and time evolution of the ion concentration in an electrophoretic cell under applied electric current.[7−9] The main advantage of MRI over electrochemical methods, such as polarization techniques, concentration cell experiments, and impedance measurements[10−12] is its ability to provide spatially resolved details about the chemical and dynamic features of charged species in solution. Therefore, such data yield a more accurate characterization of processes in an electrolyte solution under operational conditions, when compared to conventional electrochemical methods, which provide values averaged over the entire volume of the sample cell in the absence of electrodes and hence ionic currents.

By combining the *in situ* MRI experiment with inverse mathematical modeling, one can extract spatially resolved values of the salt diffusion coefficient D and the cation

Received: April 25, 2016
Published: June 2, 2016

DOI: 10.1021/jacs.6b04226
J. Am. Chem. Soc. 2016, 138, 7992−7999

transference number t^+ in Li-ion battery electrolyte solutions.[13] Mass transport in an electrolyte solution in the presence of an applied electric field occurs as a combination of migration and diffusion. For example, during the discharging of a cell, the electric field (giving rise to the ohmic potential difference in the electrolyte) causes the migration of cations to the positive electrode and anions toward the negative electrode. While Li^+ ions recombine at the positive electrode with the electrons that passed through the outer circuit, anions do not react on the electrode, and instead accumulate in the vicinity of the negative electrode. Consequently, the concentration of cations also increases near the negative electrode, in order to maintain the local electroneutrality of the electrolyte solution. This leads to the formation of an ionic concentration gradient in the electrolyte solution and to a diffusion flux opposing it. The model can be expressed by a mass-transport equation with diffusion and migration terms (eq 1a), with a uniform ion concentration as the initial condition (eq 1b), no anion flux at either electrode surface as the boundary conditions (eq 1c), and the overall system satisfying the local electroneutrality condition (eq 1d):

$$\frac{\partial c(x,t)}{\partial t} = \frac{\partial}{\partial x}\left(D(c)\frac{\partial c(x,t)}{\partial x} + \frac{J(1-t^+(c))}{F}\right) \tag{1a}$$

$$c(x,0) = c^0 \tag{1b}$$

$$\left.\frac{\partial c(x,t)}{\partial x}\right|_{x=0,L} = -\frac{J(1-t^+(c))}{D(c)F} \tag{1c}$$

$$c^+(x,t) = c^-(x,t) = c(x,t) \text{ at any } x \text{ and } t \tag{1d}$$

where c is the salt concentration, J is the electric current density, and F is Faraday's constant.

The mass-transport parameters obtained by inverse modeling with eqs 1 of the MRI measured concentration profiles in an electrophoretic cell under applied constant current are reasonable and agree with results obtained by electrochemical methods.[13] It is, however, challenging to achieve high quality MR images in the vicinity of the electrodes due to distortions of both the static (B_0) and radiofrequency magnetic fields (B_1), which are caused by the conductive parts of the cell (current collectors and the electrodes themselves).[14,15] This limitation can be overcome by optimization of the electrochemical cell design (i.e., choice of current collectors, electrodes, etc.) as well as by improvements in the MRI technique used for the visualization of the concentration profiles and by choosing favorable experimental conditions.

The concentration gradient created in the electrolyte solution of a cell that passes a constant current will continue to increase until a steady-state (time-invariant) condition is achieved, when the diffusion flux compensates for the migration flux of the ions. The diffusion flux can be represented by a linear combination of two fluxes of charged and neutral species containing the probed nucleus (^{7}Li or ^{19}F in the present case). Unfortunately, taking into account the fact that the exchange rate between different associates is within a nanosecond range,[16] it is practically impossible to distinguish between free ions and ions in neutral clusters using NMR techniques alone. Instead, pulsed field gradient NMR (PFG-NMR) yields an average value of the ionic diffusivity D_i^* represented by eq 2a, where D_i is the intrinsic diffusivity of free ions and α_i is the fraction of free ions in solution c_i/c, while D_0 and α_0 are, respectively, the diffusivity of neutral ion pairs and their fraction in the solution c_0/c ($c = c_i + c_0$).[17]

$$D_i^* = D_i\alpha_i + D_0\alpha_0 \tag{2a}$$

$$D_i\frac{\partial c_i}{\partial x} + D_0\frac{\partial c_0}{\partial x} = D_i\left(\alpha_i\frac{\partial c}{\partial x} + c\frac{\partial \alpha_i}{\partial x}\right) + D_0\left(\alpha_0\frac{\partial c}{\partial x} + c\frac{\partial \alpha_0}{\partial x}\right) \tag{2b}$$

$$D = \frac{2D_+^*D_-^*}{(D_+^* + D_-^*)} \tag{2c}$$

$$-D(c)\frac{\partial c}{\partial x} = \frac{(1-t^+(c))J}{F} \tag{2d}$$

Equation 2b shows the total diffusion flux using the definitions stated above, and evolves to a simple $D_i^*\,\partial c/\partial x$ form under the assumption that the degree of ion pairing is constant over the investigated concentration range. In that case, one can use the values of ionic diffusivities measured by PFG-NMR and the salt concentration gradient obtained directly by *in situ* MRI to describe the diffusion of ions in the electrolyte solution. Note also that the local electroneutrality condition ensures that the positive and negative ions do not move independently of each other.[18] Therefore, the salt diffusivity, which is the harmonic mean of the cation and anion diffusion coefficients measured by PFG-NMR (D_+^* and D_-^*, respectively, in eq 2c), should be used in this case.[13,19] Based on these considerations, the condition for equality between the migration and diffusion fluxes allows us to write eq 2d, which effectively describes the steady-state condition. The influence of ion pairing is also accounted for by the right-hand side of the equation, since t^+ is only proportional to the fraction of the current due to free (unassociated) cations in the electrolyte solution.

To extend the *in situ* MRI strategies presented thus far, one can combine the PFG-NMR and the MRI techniques into a single pseudo-3D experiment to determine both the salt concentration and the salt diffusivity profiles in the electrolyte solution. The lithium transference number can then be obtained by means of eq 2d from the concentration profile that exists under steady-state conditions in the presence of an applied current. The proposed procedure avoids the experimental uncertainties in the data for the regions in the immediate vicinity of the electrodes, which create difficulties for the inverse modeling analysis of MRI data. Moreover, this new method may also be applied to analysis of mass transport in dual-graphite cells, where cations intercalate into the negative electrode and anions intercalate into the positive electrode during charge.[20,21] In that case, the assumption of eq 1c is not valid, and the inverse modeling approach would require modification. In contrast, using our approach, the mass-transport parameters (both salt diffusion coefficients and the Li^+ transference numbers) are obtained from the two sets of NMR data without any further assumptions or the need for complicated mathematical computations.

The choice of a pure phase-encoding MRI technique, such as spin−echo single point imaging (SE-SPI),[22] offers many advantages for *in situ* electrochemical imaging, because it provides images free from distortions due to static field (B_0) inhomogeneity and susceptibility variations.[23] It therefore allows noticeable reductions in the previosuly mentioned uncertainties introduced by the electrodes and the conductive parts of the cell, and the collection of images significantly closer

DOI: 10.1021/jacs.6b04226
J. Am. Chem. Soc. 2016, 138, 7992−7999

to the electrodes when compared with the frequency-encoding techniques used previously for similar tasks.[7,13] The advantage of the frequency-encoding method is its—in principle—more efficient use of experimental time, because a whole line in k-space (the raw data, the Fourier transformation of which forms an actual image)[24] is collected during each scan. In contrast, only one k-space data-point can be acquired in each phase-encoded step. However, this advantage exists only for samples which do not require a large number of scans (NS) for the collection of a low noise frequency-encoded image. Furhermore, when NS is comparable to the number of pixels acquired by the phase-encoding method (32 points in our case), then the experimental time will be equal for both techiques.[25] As shown below, phase-encoding MRI allows the collection of high quality images within a reasonable recording time. In general, this technique can be used to measure local diffusivities of fluids in other nonuniform samples, e.g., any fluid-filled porous media, where frequency-encoding methods are not effective due to significant field distortions caused by the susceptibility mismatch between the fluid and the solid matrix.[26]

Herein we first validate our method with ^{7}Li and ^{19}F *in situ* MRI data by demonstrating that the distributions of cations and anions are identical in a binary symmetric electrolyte, as required by the local electroneutrality condition. Furthermore, we show that the salt concentration gradient in the electrolyte under applied constant current reaches a steady-state condition when it is proportional to the current density, as described by eq 2d. We also demonstrate, for the first time, that the pseudo-3D MRI experiment described herein allows the simultaneous measurement of the steady-state salt concentration profiles and salt diffusivity profiles in concentrated electrolyte solutions of practical interest (i.e., 0.78 to 1.27 M, for a lithium hexafluorophosphate ($LiPF_6$) solution in a binary mixture of ethylene carbonate (EC) and dimethyl carbonate (DMC) with a 1:1 volume ratio). The Li^+ cation transference number can then be determined by means of eq 2d.

EXPERIMENTAL SECTION

A 1 M $LiPF_6$/EC+DMC (1:1 v/v) electrolyte solution from Novolyte was used in the present work. The *in situ* electrophoretic cell consisted of a cell body machined from a polyether ether ketone (PEEK) rod, PEEK HPLC Super Flangeless fittings (SciPro), and two copper current collectors, one in contact with metallic lithium, the other with a composite graphite electrode deposited onto copper foil (active material density: 60 g/m^2, MTI Corporation). We have chosen a graphite electrode to avoid significant growth of dendrites on the surface of the negative electrode. It has been recently shown that, in a symmetric cell with two lithium electrodes, continuous change of the concentration gradient occurs and steady-state conditions were not reached. This was attributed to the ongoing formation of dendrites.[9]

A schematic representation of the cell is shown in Figure 1a; an electrochemical profile of graphite lithiation is shown in Figure SI-1. Cell assembly and filling with electrolyte solution were performed inside an argon-filled glovebox (0.6 ppm oxygen, <0.1 ppm water contents).

Constant current densities of 3, 6, 9, or 12 A m^{-2} (corresponding, respectively, to C/20, C/10, C/7.5, and C/5 intercalation rates for the graphite electrode used in our experiments) were applied to the cell by means of an Autolab PGStat 30 instrument operating in galvanostatic mode. The direction of the current was chosen such that lithium was stripped from the metallic Li electrode and intercalated into the top graphite electrode. Coaxial cables with grounded shields connected the cell to the potentiostat. A homemade, low-pass LC filter (with cut off frequency 2.3 MHz) prevented additional noise pick-up by the NMR probe. This measurement configuration resulted in the same MRI signal-to-noise ratio, irrespective of whether the coaxial cables were or were not connected to the cell. All experiments were carried out at 20 °C using a Bruker Avance 300 NMR spectrometer equipped with a Diff50 gradient probe and a dual resonance 8 mm ^{7}Li/^{19}F RF insert. The cell was positioned vertically inside the inset, with the B_0 field perpendicular to the electrode surfaces, while B_1 is parallel to them, such that the copper current collectors do not prevent penetration of the RF field into the electrolyte filled volume of the cell.

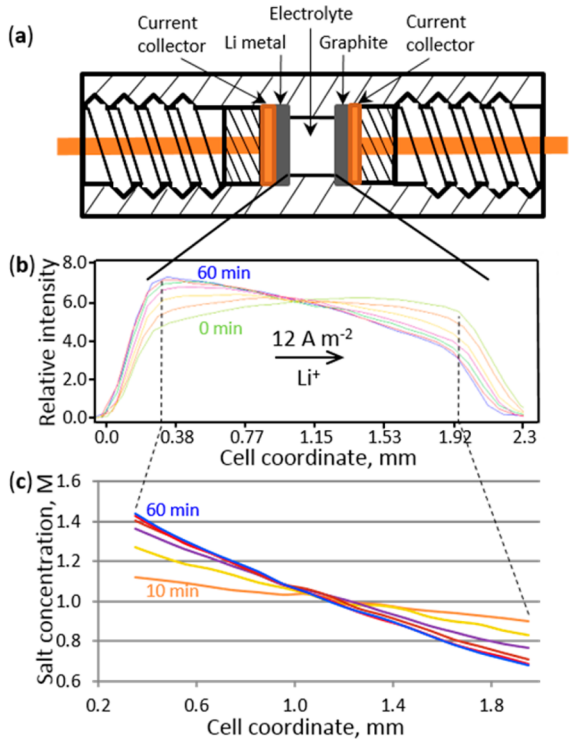

Figure 1. (a) Schematic of the *in situ* electrophoretic MRI cell design showing the cell body, the 1 M $LiPF_6$/EC:DMC (1:1 v/v) electrolyte solution, the lithium metal and graphite electrodes, the two Cu current collectors, and the seals on their respective back sides. Evolution of (b) ^{19}F MRI intensity profiles and the (c) associated anion concentration profiles under an applied current density of 12 A m^{-2}.

Two types of imaging experiments were performed in the present work. The first one is the SE-SPI, in which two scans were used for each of the 32 phase-encoding steps during which the gradient strength was increased from −15 to +15 G cm^{-1} for ^{19}F and from −37 to +37 G cm^{-1} for ^{7}Li, with a recycling delay of 5 s between subsequent scans. Echo delays were set to 1 ms for both nuclei, while transverse relaxation delays (T_2*) were estimated as 12 ms for ^{7}Li and 8 ms for ^{19}F. The total experiment duration for the collection of one image was 5 min. This technique was applied to visualize the formation of the salt concentration gradient and to study the influence of experimental parameters on the gradient under steady-state conditions. Figure 1b displays examples of ^{19}F intensity profiles along the cell axis obtained by using this method for an $LiPF_6$/EC:DMC (1:1 v/v) electrolyte solution with 1 M initial salt concentration, which developed in the presence of an applied electric current density of 12 A m^{-2}. The images were collected during 1 h, at 10 min intervals. The ion concentration at any particular point of the sample can be calculated from the measured profiles by normalizing the images with respect to the data obtained in the absence of the electric current, under the assumption of a uniform initial salt distribution. Such a normalization effectively eliminates image distortions caused by the spatial variation of the B_1 field, which is intrinsic to any probe and is constant during the experiment.

For the second type of experiment, we substituted the 90° pulse in the spin−echo chemical shift imaging[27] with the one-shot diffusion-ordered NMR spectroscopy pulse sequence, which utilizes asymmetric

DOI: 10.1021/jacs.6b04226
J. Am. Chem. Soc. 2016, 138, 7992−7999

gradients rather than a full phase cycle, to more rapidly acquire the diffusion data sets.[28] In this pseudo-3D experiment, the three orthogonal projections correspond to the chemical shift, the diffusion coefficient, and the spatial distribution of the ionic species in the solution (Figure 4). Eight scans were collected for each of the 16 phase-encoding steps (-7.5 G cm^{-1} < $G_I(^{19}F)$ < 7.5 G cm^{-1}, -18.5 G cm^{-1} < $G_I(^{7}Li)$ < 18.5 G cm^{-1}) and 8 increments of diffusion encoding gradient (G_D) (up to 47 G cm^{-1} for ^{19}F and 158 G cm^{-1} for ^{7}Li), with an imbalance factor (α) of 0.2, diffusion time of 100 ms, gradient pulse length of 1 ms, and spoiling gradient strength (G_S) of 30 G cm^{-1} (Figure 4). The total duration of this experiment was 35 min. Further details on the implementation of the pulse sequence are available in the Supporting Information. Ion diffusion coefficients for each spatial data point (an axial profile through the cell) were obtained from fits of the signal attenuation to the parameters of the pulse sequence as described by Pelta et al.[28] The accuracy of the diffusion coefficients measured by PFG-NMR was estimated as ±1%, based on the fit quality.

RESULTS AND DISCUSSION

^{19}F *in situ* MR images obtained for the 1 M $LiPF_6$/EC:DMC 1:1 v/v electrolyte solution under the application of an electric current density of 12 A m^{-2} are shown in Figure 1b. The signal intensity at any point along the cell coordinate corresponds to the anion concentration in that particular slice along the cell axis. Note that the image obtained without an applied current (green line in Figure 1b, corresponding to t = 0) deviates from the expected rectangular shape based on the cell geometry. Deviations from the ideal shape can be attributed (i) to the inhomogeneity of the radio frequency field strength (which causes the rounded (convex) profile away from the electrodes) and (ii) to the influence of the metallic current collectors (which attenuate the signal in the vicinity of the electrode surfaces, i.e., at distances <0.4 mm).[29] We expect, however, that the B_1 inhomogeneity is constant over the duration of the experiment. Therefore, its impact can be effectively eliminated by normalizing all of the images obtained with an applied current to the t = 0 image, corresponding to zero current, and hence to a uniform concentration throughout the cell, to obtain the concentration profiles shown in Figure 1c. As shown in Figure SI-4 the attenuation of the signal near the electrodes causes a significant decrease in signal-to-noise ratio (increased experimental error). Therefore, the regions of the cell within a distance of 0.37 mm from either electrode (marked by vertical dashed lines in Figure 1b) were excluded from the data analysis, i.e., were not used in the determination of the mass-transport parameters.

One of the key aims for this study was to develop a technique, including cell design, to accurately describe the behavior of the electrolyte solution under conditions similar to those existing in commercial batteries and to place the electrodes as close together as possible. The latter is particularly challenging due to the strong inhomogeneity of the magnetic field in the vicinity of metallic current collectors. Frequency-encoding was used in all previously published *in situ* MRI investigations of electrolytes.[7,8,13] Note that this technique is highly sensitive to magnetic field inhomogeneities. Therefore, the electrolyte could not be probed reliably at distances less than 2 mm from each electrode when the total interelectrode distance varied between 1 and 2 cm. Moreover, since the time required for the development of the steady-state depends on the distance between the electrodes, no steady-state was reached even after 16 h of applied current at such electrode separations. The main difference in the present study is the application of a phase-encoding MRI technique, which provides images free from the distortions caused by B_0 inhomogeneity and susceptibility variations. Therefore, the electrodes can be placed closer to each other. (The electrode spacing for the cell shown in Figure 1a is 2.3 mm.) As can be seen from Figures 1b and 1c, the anion concentration profiles change continuously during the first 40 min of the experiment and then reach steady-state. Since in a real battery the electrodes are positioned one hundred times closer to each other (with a 10 to 25 μm spacing), the behavior of the electrolyte solution in the battery of an electrified vehicle under operational conditions can be represented as a series of steady-states with rapid changes in the concentration gradient in response to changes in the applied current. Performing such MRI experiments over length scales relevant for batteries (i.e < 0.1 mm interelectrode spacing) would also be of interest. In that case, the structural features of the electrode material, such as porosity and tortuosity, may play a role in electrolyte transport. However, further development of the apparatus and techniques is required to achieve this goal. Herein we focus on the properties of the bulk electrolyte solution, assuming that they are independent of the transport within the electrodes.

In the present study, our first objective was to validate our method by verifying the identity of the concentration profiles for cations and anions in a binary symmetric electrolyte, as required by the local electroneutrality condition. This was accomplished with a dual tuned $^{7}Li/^{19}F$ RF insert, which allowed a direct comparison of the cation and anion axial concentration profiles obtained from the ^{7}Li and ^{19}F images, as shown in Figure 2. As expected, the two concentration profiles

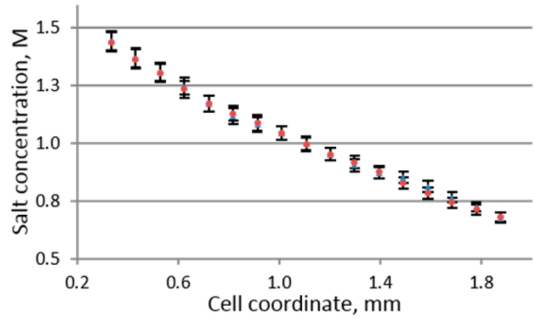

Figure 2. Concentration profiles of ^{7}Li (maroon circles) and ^{19}F (blue triangles) obtained in 1 M $LiPF_6$/EC:DMC 1:1 v/v 1 h after applying a current density J = 12 A m^{-2}.

are identical within the experimental error of 3% (estimated from the signal-to-noise ratio in the images). Therefore, in the case of binary symmetric electrolytes, the choice of ion to be tracked is dictated solely by considerations that create optimal experimental conditions. (In the present case, the relative NMR sensitivity for the ^{19}F nucleus is ~3 times higher than that for ^{7}Li; hence, monitoring the ^{19}F nucleus is preferable for monitoring the ^{7}Li nucleus.) For multi-ion solutions, such as lithium salt solutions in ionic liquids,[30] or mixed-anion electrolytes,[31] MRI can provide ion-specific information about the distribution of species in solution, which represents a significant advantage over electrochemical methods for determining diffusion coefficients and transference numbers.

In order to verify the influence of the applied electric current on the salt concentration gradient under steady-state conditions, we carried out an experiment in which the current

DOI: 10.1021/jacs.6b04226
J. Am. Chem. Soc. 2016, 138, 7992−7999

was increased stepwise. The initial current density was 3 A m^{-2}, and several identical images were collected after the transient period of steady-state gradient formation, to verify that the ionic concentration profile in the electrolyte had reached the steady-state. The current density was then doubled to 6 A·m^{-2} and new images were acquired, followed by yet another doubling to 12 A·m^{-2}. The steady-state concentration profiles obtained at 3, 6, and 12 A·m^{-2} are shown in Figure 3a. As

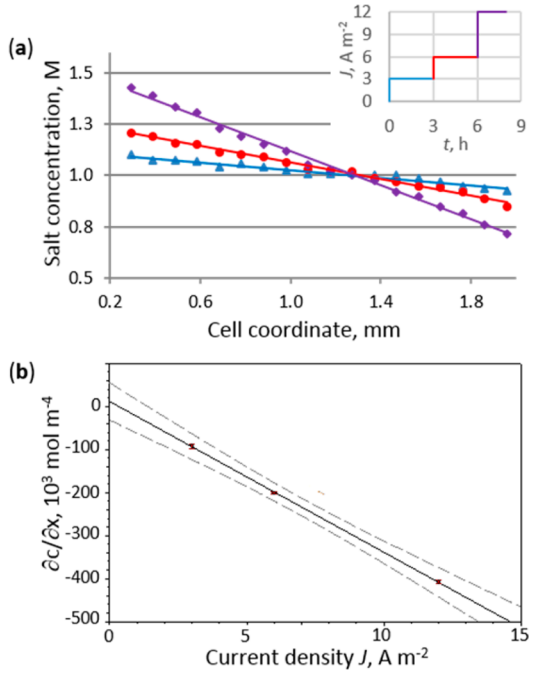

Figure 3. (a) Steady-state lithium salt concentration profiles at current densities of 3 (blue triangles), 6 (red circles), and 12 (purple rhombs) A m^{-2} (changes of current regimes are shown in the top right corner inset). Linear fits of the data are given by the solid lines. (b) Depedence of the steady-state salt concentration gradients on the applied current density. Regression line: $\partial c/\partial x$ = 11.5−35.02 J; R^2 = 0.9994; the dashed lines represent 95% confidence intervals.

expected, the salt concentration gradient increases with increasing electric current. The value of $\frac{\partial c}{\partial x}$ can be estimated under the assumption of a constant diffusivity and transference number. In this case, a linear fit of the data points gives values of the concentration gradient equal to $-(0.92 \pm 0.05) \times 10^5$, $-(2.01 \pm 0.02) \times 10^5$, and $-(4.08 \pm 0.04) \times 10^5$ mol·m^{-4} for J = 3, 6, and 12 A·m^{-2}, respectively. While these estimates are somewhat crude, since mass-transport properties (especially D) are concentration-dependent,[13,32] one can see nevertheless that there exists proportionality between $\frac{\partial c}{\partial x}$ and J, as displayed in Figure 3b and expected from eq 2d. The R^2 value of 0.9998 for the linear regression in Figure 3b indicates excellent linearity. The value of 11.5 (instead of zero) for the ordinate at the origin is within the 95% confidence limits, represents only ∼3% of the gradient values' variation range, and is of similar size as the uncertainty for the gradient values. This is likely a consequence of ignoring the salt concentration dependencies for the salt diffusion coefficient and lithium transference number. Nevertheless, the excellent linearity serves as the internal validation of the degree of ion pairing invariance required to connect the NMR and MRI data with the applied current density by eqs 2.

A pseudo-3D experiment was employed for a more detailed characterization of mass transport in the electrolyte solution. In the spectrum thus obtained, the three orthogonal projections correspond to the chemical shift, the diffusion coefficient, and the spatial distribution of the ionic species in the solution (Figure 4). As expected, in the absence of an electric current, the concentration distribution of the salt in the electrolyte is highly uniform and the salt diffusion coefficient was determined to be $(2.33 \pm 0.07) \times 10^{-10}$ m^2 s^{-1} (see Figure SI-3). This value agrees well with our results obtained for the same solution from a PFG-NMR measurement (see Supporting Information) and thus validates the pseudo-3D pulse program design.

The salt diffusivity and Li^+ transference number were simultaneously determined from the steady-state concentration gradient developed at a constant current density of 9 A m^{-2}. The salt concentration profile developed in the cell in this state and the corresponding salt diffusivity are displayed in Figure 5. Their values together with the Li^+ transference number are also listed in Table 1. It should be mentioned that these experiments were carried out with 4 times the number of scans per each gradient increment used in the SE-SPI measurements shown in Figures 2 and 3. Therefore, the signal-to-noise ratio and, consequently, the accuracy of the salt concentration measurements are both higher (the experimental error is 1% with this number of scans). A second order polynomial was used to fit the data (Figure 5) and to determine the numerical values of the concentration gradient at each point in the cell. It is readily visible from Figure 5 that the salt diffusivity has a significant dependence on salt concentration, with values of D measured at opposite ends of the cell varying by more than 60% corresponding to a change in the salt concentration range from 0.78 M to 1.27 M. This conclusion is in good agreement with our previous results, which were obtained by *in situ* slice-selective NMR diffusion measurements.[32] Moreover, this spatially resolved profile of the concentration gradient is evaluated over a distance smaller than 2 mm.

Note also that the diffusion coefficient measured at 1 M under steady-state conditions agrees well (within the experimental error) with the value obtained for the same electrolyte solution in the absence of an applied current. Furthermore, this observation is in agreement with the fact that randomly oriented instantaneous velocities of ions undergoing Brownian motion are several orders of magnitude higher than the migration velocities generated by the applied electric field.[33] Moreover, it is also supported by the fact that the ions in the solution screen the potential of the electrode over a length scale given by the Debye length, which is on the nanometer scale for electrolyte solutions at concentrations of practical interest.[34] In essence, this finding shows that the concentration is the primary variable determining the diffusivity at any place in the cell. This speaks to the value of the newly proposed *in situ* MRI approach, as the concentration profile alone provides the necessary input for determining the mass-transport parameters. Our novel methodology can be used to evaluate concentration profiles and the spatial distribution of the salt diffusivity under any set of electrochemical test conditions. These data, when paired with *ex situ* conductivity measurements carried out with electrolyte solutions of the same salt concentrations as those detected by *in situ* MRI, could provide full data on the degree of ion pairing for a complete model of mass transport.

The lithium transference number is known to be significantly less dependent on salt concentration than the salt diffusivity.[13,35] Typically, the variation is within several percent over

DOI: 10.1021/jacs.6b04226
J. Am. Chem. Soc. 2016, 138, 7992−7999

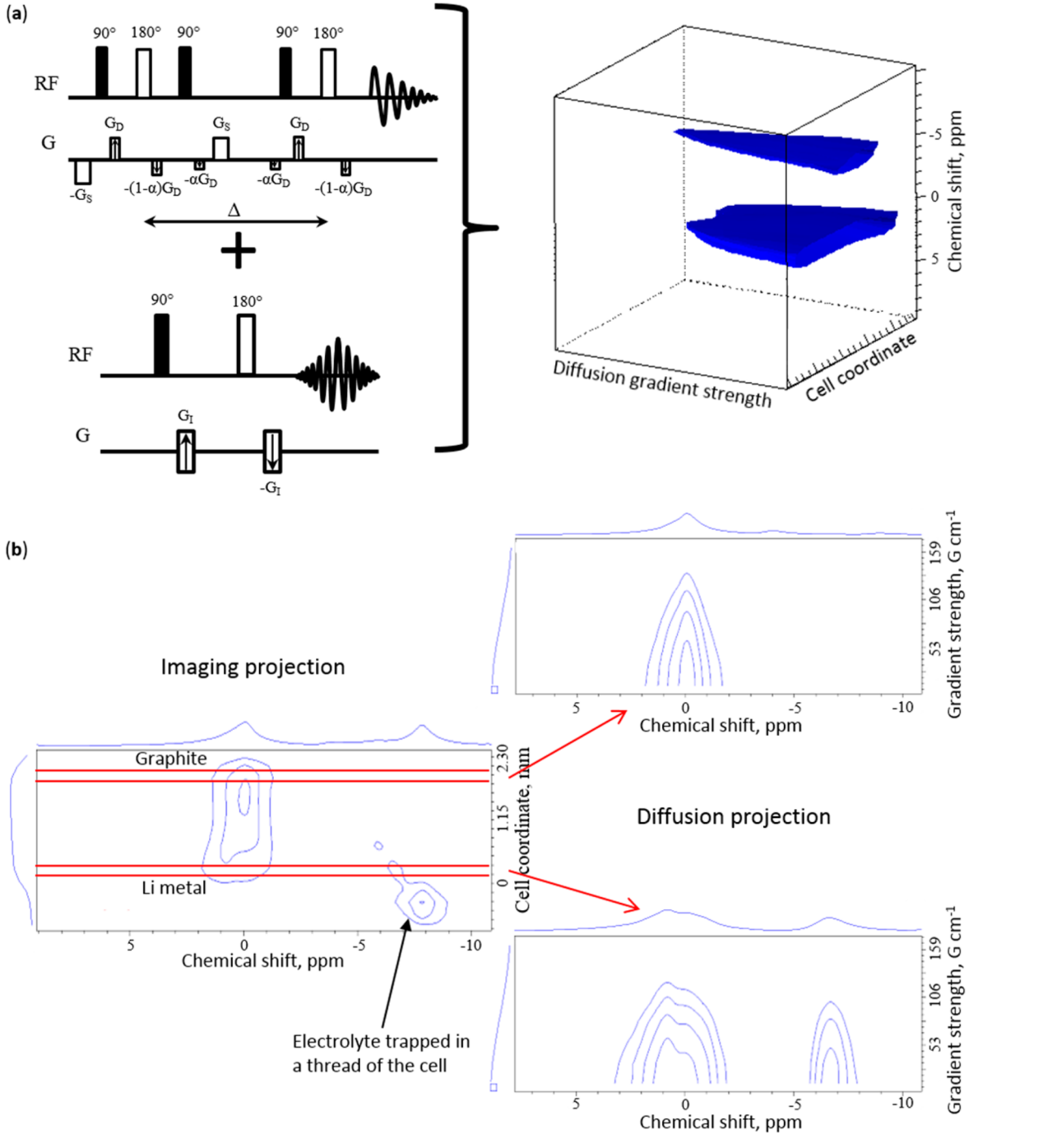

Figure 4. (a) Schematic representation of the pseudo-3D experiment design, with RF and gradient pulses labeled as described in the Experimental Section. (b) 2D projections of the obtained 3D spectrum. The spectral window in the imaging direction selects only the active volume between the two electrodes, in order to maximize the resolution in the probed region. This resulted in a spurious signal of the electrolyte trapped in the threads of the cell being folded into the image, observable at −7 ppm. This signal was not considered during postprocessing of the spectrum.

the concentration range 0.5−1.5 M. This is within the experimental error defined by propagation of the errors of measured parameters (ionic diffusivities and salt concentration) and by the fact that t^+ is calculated by eqs 2. Values of the lithium transference number obtained from the experimentally derived D and c distributions are shown in Table 1. There is a slight trend toward the increase of t^+ with decreasing concentration, which can be explained by the decreasing of ion pairing at lower c;[36] however, with the exception of the lowest concentration data point, all of the obtained values lie within the experimental error with $t^+ = 0.31 \pm 0.03$.

■ CONCLUSIONS

In this study we have demonstrated for the first time that, using the *in situ* MRI technique, one can image the formation of steady-state concentration gradients in an operating Li-ion battery, that is, when the diffusion flux of ions in the formed salt concentration gradient completely compensates the migration fluxes of the ions. By combining MRI with the PFG-NMR

DOI: 10.1021/jacs.6b04226
J. Am. Chem. Soc. 2016, 138, 7992−7999

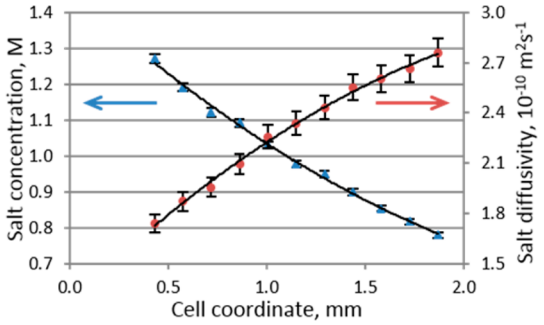

Figure 5. Steady-state lithium salt concentration (blue triangles) and diffusivity (maroon circles) profiles in 1 M $LiPF_6$/EC:DMC (1:1 v/v) at a current density of 9 A m^{-2}.

Table 1. Concentration Dependences of the Salt Diffusivity and Lithium Transference Numbers Obtained from the *in Situ* MRI Experiment under Steady-State Conditions with an Applied Current Density of 9 A·m^{-2}

c, M	D, 10^{-10} m^2/s	t^+
1.27 ± 0.01	1.74 ± 0.05	0.30 ± 0.03
1.19 ± 0.01	1.87 ± 0.06	0.29 ± 0.03
1.12 ± 0.01	1.96 ± 0.06	0.29 ± 0.03
1.09 ± 0.01	2.09 ± 0.06	0.28 ± 0.03
1.03 ± 0.01	2.26 ± 0.07	0.29 ± 0.03
0.98 ± 0.01	2.34 ± 0.07	0.30 ± 0.03
0.95 ± 0.01	2.43 ± 0.07	0.30 ± 0.03
0.898 ± 0.009	2.55 ± 0.08	0.32 ± 0.03
0.854 ± 0.009	2.60 ± 0.08	0.33 ± 0.03
0.817 ± 0.008	2.67 ± 0.08	0.34 ± 0.03
0.780 ± 0.008	2.76 ± 0.08	0.35 ± 0.03

diffusion measurements, one can simultaneously obtain information about the distributions of the ions and their diffusivities in solution. Furthermore, by using those data and the equation of mass transport under steady-state conditions, it is also possible to determine the lithium transference number for the electrolyte solution. The effectiveness of the method was demonstrated for a 1 M $LiPF_6$/EC:DMC 1:1 v/v electrolyte composition.

■ ASSOCIATED CONTENT

Supporting Information

The Supporting Information is available free of charge on the ACS Publications website at DOI: 10.1021/jacs.6b04226.

Voltage profile of graphite lithiation in the *in situ* cell, PFG-NMR diffusion measurement on the bulk electrolyte, pulse sequence parameters and spatially resolved diffusion coefficients obtained in the *in situ* cell in the absence of an applied electric current, and concentration profiles without trimming of areas close to electrodes (PDF)

■ AUTHOR INFORMATION

Corresponding Author

*goward@mcmaster.ca

Notes

The authors declare no competing financial interest.

■ ACKNOWLEDGMENTS

The authors are grateful to Bryce MacMillan and Klaus Zick for helpful discussions regarding MRI techniques, and they thank Bob Powell for a careful reading of the manuscript and excellent editorial suggestions. They also acknowledge funding through the NSERC Strategic grant program, GM of Canada and Bruker BioSpin Canada.

■ REFERENCES

(1) Tanim, T. R.; Rahn, C. D.; Wang, C.-Y. *J. Dyn. Syst., Meas., Control* **2015**, *137*, 011005.
(2) Nyman, A.; Zavalis, T. G.; Elger, R.; Behm, M. r.; Lindbergh, G.Rr. *J. Electrochem. Soc.* **2010**, *157*, A1236.
(3) Ilott, A. J.; Trease, N. M.; Grey, C. P.; Jerschow, A. *Nat. Commun.* **2014**, *5*, 4536.
(4) Salager, E.; Sarou-Kanian, V.; Sathiya, M.; Tang, M.; Leriche, J.-B.; Melin, P.; Wang, Z.; Vezin, H.; Bessada, C.; Deschamps, M.; Tarascon, J.-M. *Chem. Mater.* **2014**, *26*, 7009.
(5) Zhang, Z.; Martin, J.; Wu, J.; Wang, H.; Promislow, K.; Balcom, B. J. *J. Magn. Reson.* **2008**, *193*, 259.
(6) Chandrashekar, S.; Trease, N. M.; Chang, H. J.; Du, L. S.; Grey, C. P.; Jerschow, A. *Nat. Mater.* **2012**, *11*, 311.
(7) Klett, M.; Giesecke, M.; Nyman, A.; Hallberg, F.; Lindstrom, R. W.; Lindbergh, G.; Furo, I. *J. Am. Chem. Soc.* **2012**, *134*, 14654.
(8) Klamor, S.; Zick, K.; Oerther, T.; Schappacher, F. M.; Winter, M.; Brunklaus, G. *Phys. Chem. Chem. Phys.* **2015**, *17*, 4458.
(9) Chang, H. J.; Ilott, A. J.; Trease, N. M.; Mohammadi, M.; Jerschow, A.; Grey, C. P. *J. Am. Chem. Soc.* **2015**, *137*, 15209.
(10) Zugmann, S.; Fleischmann, M.; Amereller, M.; Gschwind, R. M.; Wiemhöfer, H. D.; Gores, H. J. *Electrochim. Acta* **2011**, *56*, 3926.
(11) Li, L. F.; Lee, H. S.; Li, H.; Yang, X. Q.; Nam, K. W.; Yoon, W. S.; McBreen, J.; Huang, X. J. *J. Power Sources* **2008**, *184*, 517.
(12) Zhao, J.; Wang, L.; He, X.; Wan, C.; Jiang, C. *J. Electrochem. Soc.* **2008**, *155*, A292.
(13) Sethurajan, A. K.; Krachkovskiy, S. A.; Halalay, I. C.; Goward, G. R.; Protas, B. *J. Phys. Chem. B* **2015**, *119*, 12238.
(14) Romanenko, K.; Forsyth, M.; O'Dell, L. A. *J. Magn. Reson.* **2014**, *248*, 96.
(15) Vashaee, S.; Goora, F.; Britton, M. M.; Newling, B.; Balcom, B. J. *J. Magn. Reson.* **2015**, *250*, 17.
(16) Borodin, O.; Smith, G. D. *J. Phys. Chem. B* **2009**, *113*, 1763.
(17) Stolwijk, N. A.; Kosters, J.; Wiencierz, M.; Schoenhoff, M. *Electrochim. Acta* **2013**, *102*, 451.
(18) Mills, R.; Lobo, V. M. M. *Self-diffusion in electrolyte solutions: a critical examination of data compiled from the literature*; Elsevier: New York, NY, USA, 1989.
(19) Georén, P.; Lindbergh, G. *Electrochim. Acta* **2004**, *49*, 3497.
(20) Placke, T.; Fromm, O.; Lux, S. F.; Bieker, P.; Rothermel, S.; Meyer, H. W.; Passerini, S.; Winter, M. *J. Electrochem. Soc.* **2012**, *159*, A1755.
(21) Qi, X.; Blizanac, B.; DuPasquier, A.; Meister, P.; Placke, T.; Oljaca, M.; Li, J.; Winter, M. *Phys. Chem. Chem. Phys.* **2014**, *16*, 25306.
(22) Ouriadov, A. V.; MacGregor, R. P.; Balcom, B. J. *J. Magn. Reson.* **2004**, *169*, 174.
(23) Gravina, S.; Cory, D. G. *J. Magn. Reson., Ser. B* **1994**, *104*, 53.
(24) Ljunggren, S. *J. Magn. Reson.* **1983**, *54*, 338.
(25) Callaghan, P. T.; Forde, L. C.; Rofe, C. J. *J. Magn. Reson., Ser. B* **1994**, *104*, 34.
(26) Li, L.; Chen, Q.; Marble, A. E.; Romero-Zeron, L.; Newling, B.; Balcom, B. J. *J. Magn. Reson.* **2009**, *197*, 1.
(27) Brown, R. W.; Cheng, Y. C. N.; Haacke, E. M.; Thompson, M. R.; Venkatesan, R. *Magnetic Resonance Imaging: Physical Principles and Sequence Design*; Wiley: Hoboken, NJ, USA, 2014.
(28) Pelta, M. D.; Morris, G. A.; Stchedroff, M. J.; Hammond, S. J. *Magn. Reson. Chem.* **2002**, *40*, S147.
(29) Hoult, D. I. *Prog. Nucl. Magn. Reson. Spectrosc.* **1978**, *12*, 41.
(30) Armand, M.; Endres, F.; MacFarlane, D. R.; Ohno, H.; Scrosati, B. *Nat. Mater.* **2009**, *8*, 621.

DOI: 10.1021/jacs.6b04226
J. Am. Chem. Soc. 2016, 138, 7992−7999

(31) Zaidi, W.; Boisset, A.; Jacquemin, J.; Timperman, L.; Anouti, M. *J. Phys. Chem. C* **2014**, *118*, 4033.
(32) Krachkovskiy, S. A.; Pauric, A. D.; Halalay, I. C.; Goward, G. R. *J. Phys. Chem. Lett.* **2013**, *4*, 3940.
(33) Price, W. S. *NMR Studies of Translational Motion: Principles and Applications*; Cambridge University Press: Cambridge, UK, 2009.
(34) Kohonen, M. M.; Karaman, M. E.; Pashley, R. M. *Langmuir* **2000**, *16*, 5749.
(35) Aihara, Y.; Bando, T.; Nakagawa, H.; Yoshida, H.; Hayamizu, K.; Akiba, E.; Price, W. S. *J. Electrochem. Soc.* **2004**, *151*, A119.
(36) Dai, H.; Zawodzinski, T. A. *J. Electroanal. Chem.* **1998**, *459*, 111.

DOI: 10.1021/jacs.6b04226
J. Am. Chem. Soc. 2016, 138, 7992−7999